Understanding the evolution of syn-depositional folds: coupling decompaction and 3D sequential restoration

Pauline Durand-Riard[*][†], Lise Salles[*], Mary Ford[*],
Guillaume Caumon[*]and Jeanne Pellerin[*]

Abstract

The analysis of basin dynamics and burial evolution requires a good understanding of sediment compaction. Classically, decompaction of sediments is performed in one dimension at a well location, using either a simple compaction/depth relationship or more complex elasto-plastic models. This paper presents a new approach combining sequential decompaction with 3D restoration to allow for a true 3D basin analysis. Decompaction is performed in 3D after each restoration step, thus taking into account possible tectonic events and lateral thickness variations. Care is taken to apply decompaction to ensure volume continuity especially around faults. This approach is particularly suitable for syn-depositional folds whose growth strata constrain tectonic evolution through time.

The proposed approach is applied to the sand-rich turbiditic reservoir analogue of Annot (SE France) where two fictitious wells are used to compare the new 3D technique to a well decompaction analysis. Coupling restoration and decompaction leads to an improved assessment of the basin history: an uplift of the underlying units is identified, which was not detected using decompaction on wells only. Such differences may have a significant impact on possible hydrocarbon maturation models of the basin. Moreover, the geometry of the restored and decompacted models can better constrains the basin history, and influence our understanding of potential hydrocarbon migration pathways.

[*]CRPG - Nancy-Université
[†]Email: durandriard@gocad.org

1 Introduction

Subsidence analysis based on decompaction curves is a standard method in sedimentary basin investigation [Sclater and Christie, 1980, Maillard et al., 2003, Gutierrez and Wangen, 2005, Hölzel et al., 2008]. Sediment compaction affects petrophysical properties in a sedimentary basin, such as pressure, porosity and permeability. It can also affect the basin history itself. For example, compaction may lead to salt diapirism in the absence of tectonic events [Maillard et al., 2003]. It is therefore of importance to account for compaction in basin analysis. Several models of decompaction have been developed, based on two main approaches: the "classical" method, which considers compaction as a function of depth and rock types [Weller, 1959, Magara, 1976, McKenzie, 1978, Sclater and Christie, 1980, Schmoker and Halley, 1982, Lerche, 1990a, Gutierrez and Wangen, 2005], and the elasto-plastic approach, requiring more geological and physical parameters to constrain progressive decompaction [Schneider et al., 1996]. In 3D, decompaction should also relate to tectonic deformation, especially in structurally complex areas. Syn-tectonic deposits play a key role in assessing the structural evolution of a basin, hence providing essential information for compaction analysis.

In parallel, balanced restoration, which aims at retro-deforming sedimentary layers back to a horizontal datum or a known depositional state, is a fundamental tool in structural geology [Chamberlin, 1910, Dahlstrom, 1969, Groshong, 1999]. In 3D, recent authors [Muron, 2005, Maerten and Maerten, 2006, Moretti et al., 2006, Durand-Riard et al., 2010] treat sequential restoration as a geomechanical problem constrained by displacement boundary conditions, contact conditions, geomechanical rock properties and behavioral laws. Restoration, performed using a finite element method, provides the displacement field for the whole model, allowing an accurate estimation of depth changes during basin depositional history. Furthermore, the amount of eroded material can be estimated and unconformities can be conveniently handled by using "implicit" stratigraphic models [Durand-Riard et al., 2010], where the mesh is conformable only to faults [Caumon et al., 2007, Frank et al., 2007].

The objective of this paper is to couple decompaction and sequential restoration in 3D to have a better understanding of basin burial history, as illustrated in Fig.1. We apply this new technique to the Annot Sandstone Formation in the Annot growth syncline (SE France) to illustrate the impact of taking into account deformation history during backstripping, as well as highlighting the importance of the decompaction.
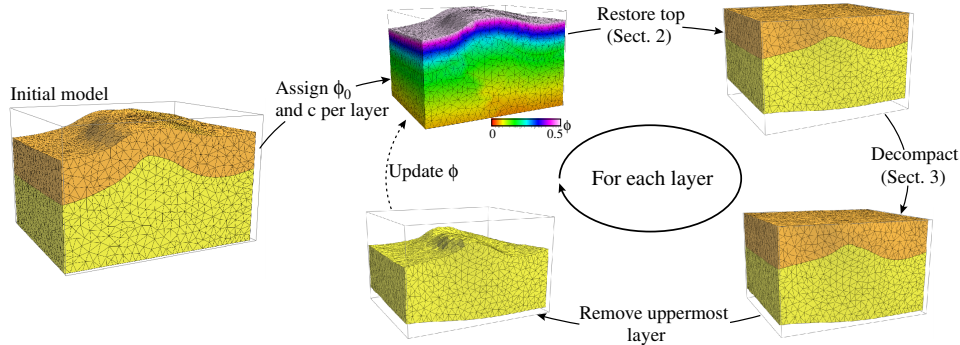
Figure 1: Flowchart of restoration and decompaction, applied to a syn-depositional anticline (2 layers). For each layer: the porosity ϕ is assigned according to the layer's lithology and varies with depth; the topmost layer is restored; the model is decompacted; the restored layer is removed; and the porosity ϕ is updated as a function of the new depth. Then, the process can be applied to the next layer.

2   Decompacting stratigraphic piles

2.1   The main approaches

The first decompaction models were proposed by Athy [1930], before being enhanced by several authors [Weller, 1959, Magara, 1976, Sclater and Christie, 1980, Schmoker and Halley, 1982, Lerche, 1990a, Gutierrez and Wangen, 2005]. These approaches assume that normally pressured sediments exhibit an exponential relationship between depth and porosity of the form:

$$\phi = \phi_0.\exp(-cZ) \qquad (1)$$

where ϕ is the porosity at any depth Z, ϕ_0 is the porosity at the time of deposition and c is an internal coefficient dependent on lithology (Fig.2).

This classical analytical approach assumes that the load-response compaction rate has been constant through time, and that the vertical solid volume was constant. However, as discussed in Allen and Allen [2005], in nature, these conditions rarely occur. Many factors may affect this porosity-depth relationship, such as lithology, depositional facies, composition of framework grains, temperature, and time. Erosion, tectonics, chemical phenomena and fluid pressure can also affect compaction [Makhous, 2000]. Various authors [Weller, 1959, Sclater and Christie, 1980, Schmoker and Gautier, 1989, Lerche, 1990b, Hölzel et al., 2008] have proposed a variety of more detailed porosity-depth relations, each based on a similar principle of porosity destruction under the increasing effective stresses experienced during burial.

The elasto-plastic approach better constrains decompaction and provides a more accurate physical model, as it also accounts for fluid pressure. Schnei-
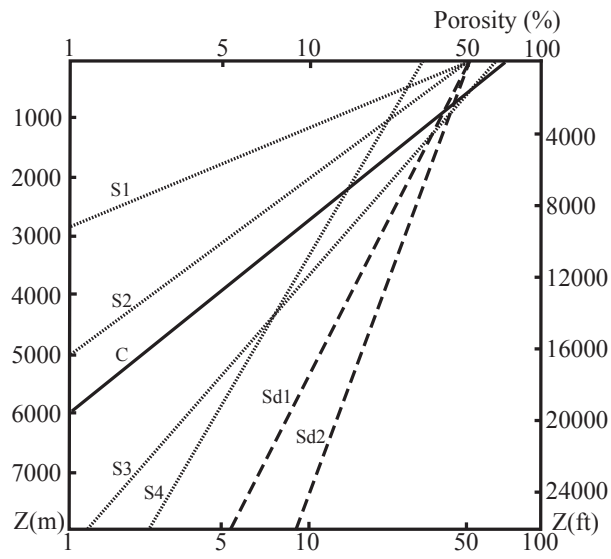
Figure 2: Variation of the present-day porosity as a function of the maximum burial depth (Z) for different lithologies, compiled from several sources: C: Chalk [Sclater and Christie, 1980]; S: Shales from 1: Athy [1930], 2: Hedberf [1936], 3: Sclater and Christie [1980], and 4: Dickinson [1953]; Sd: Sandstones from 1: Sclater and Christie [1980] and 2: Atwater and Miller [1965]. Note that shales compact quickly compared to sandstones.

4

der et al. [1996] express elasto-plastic decompaction with a system of five equations, involving about twenty parameters including time t, porosity ϕ, permeability k, phase velocities V of water and solid, pore fluid pressure q, lithostatic pressure P, stress σ, gravity g, rock density ρ, and viscosity μ. Mineralization, hydrocarbon generation or heat flow may affect compaction and thus bias the model [Magara, 1980, Fowler and Noon, 1999, Makhous, 2000, Suetnova, 2007]. Adding parameters such as pore elasto-plasticity could also lead to very different results from the standard elasto-plastic approach [Yarushina and Podladchikov, 2007].

However, the large number of required parameters for the elasto-plastic approach makes it difficult to apply, in particular during early stages of basin exploration when the basin parameters are poorly constrained. In contrast, in order to apply the classical approach, only surface porosity and compaction coefficient are required. In exploration, surface porosity is generally poorly known in a basin, but can be found in literature; it can also be measured in boreholes and extrapolated. Surface porosity can be assigned according to unit lithology. Moreover, Shneider et al. [1994] admit that an elasto-plastic approach is valid only in the sedimentary basin subsurface or in areas where the porosity is low. In subsurface, elasto-plastic and classical models thus lead to similar results [Perez, 1998].

2.2 One-dimension decompaction limits

Most authors apply decompaction methods to wells in order to analyse the subsidence history of a basin [Athy, 1930, Weller, 1959, Sclater and Christie, 1980, Magara, 1976, Hegarty et al., 2007, Pearson and Russel, 2000, Nelskamp et al., 2008]. Notwithstanding assumptions about the depth-porosity relationship, the computation of decompaction along well paths can give biased results because tectonic deformation between wells may have great importance. A true 3D analysis could shed some light on this process. In several recent modelling tools, subsidence calculations, thickness variations and depth changes are assessed using Monte-Carlo simulations [Meckel et al., 2007, Hölzel et al., 2008], but this process may lead to unrealistic results. Moreover, it cannot account for unconformities that may affect layers. In order to address these issues, we use 3D sequential restoration results as an input for a true 3D decompaction, taking into account erosional events and thickness variations.

3 Restoring volumetric models

3.1 From kinematic to geomechanical restoration

Cross-section restoration was first conceived by Chamberlin [1910], and then formalized by Dahlstrom [1969], before being extended to map restoration

[Dahlstrom, 1969, Gibbs, 1983, Gratier and Guillier, 1993, Rouby, 1994, Rouby et al., 2000]. The method restores sedimentary layer boundaries back to their pre-deformation geometry, usually assuming a flat and horizontal depositional configuration. Most of these restoration methods are purely kinematic, based on geometric assumptions such as length, angle or area conservation. Consequently, these techniques do not account for rock behavioural laws, relating deformation and stress, and do not consider contrasts in rock geomechanical properties. In the case of complex geological structures including fault propagation folds and fault bend folds, the description of the displacement and strain fields is not accurate. In such cases, volumetric mechanical restoration methods can provide better accuracy in the description of strain and stress fields [De Santi et al., 2002, Muron, 2005, Maerten and Maerten, 2006, Moretti et al., 2006, Moretti, 2008, Durand-Riard et al., 2010].

3.2   Performing 3D geomechanical restoration

To perform 3D restoration, an elastic behavioral law is assigned to the model and isotropic rock properties are defined for each layer. Displacement boundary conditions are defined: (i) the topmost horizon is set to a reference elevation; (ii) some regions of the model are fixed to avoid body rotation and ensure the uniqueness of the solution. Contact conditions are set to ensure there are neither gaps nor overlaps between fault blocks at the end of the restoration. Then, the finite element method is used to compute the displacement field while honouring boundary conditions, minimizing the energy of deformation and respecting moment and mass preservation principles [Muron, 2005, Durand-Riard et al., 2010, Durand-Riard, 2010]. Volume variation is minimized during this process, but the restored state can have local volume changes due to retro-deformation of the model.

Restoration is performed sequentially on each layer of the model, from top to bottom, and leads to the retro-deformation tensor, from which retro-strain and retro-dilation are computed. For the sake of simplicity, in the following sections, deformation, strain and dilation are used instead of, respectively, retro-deformation, retro-strain and retro-dilation.

In order to avoid meshing issues in thin layers, we use the new restoration technique developed by Durand-Riard et al. [2010], where the restoration is applied to implicit models, in which horizons are represented as a scalar property isovalue in the tetrahedral model [Frank et al., 2007]. Because the properties representing horizons are continuous through the whole model, unconformities are dealt with easily, and eroded volumes can be reconstructed between successive restoration steps.
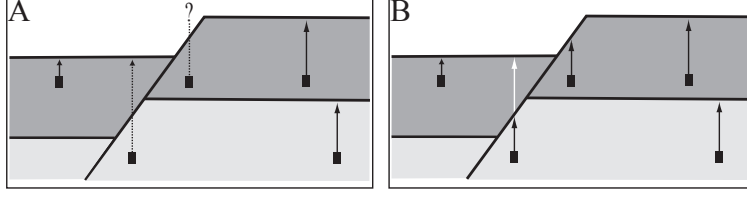
Figure 3: Projection onto a reference surface. A: Using stratigraphic upper surfaces, compaction may be computed in a multi-lithological column except in the case of a fault; B: Using mathematical tops, compaction can be computed correctly.

4 Integrating decompaction into the 3D restoration process

4.1 Method

Performing sequential restoration on a geological subsurface model leads to an improved understanding of the basin history, but in most cases decompaction is not incorporated. We propose to include decompaction into the restoration process in order to assess the basin history in a more complete way. Depth changes derived from restoration, with respect to a base level, are used as input for decompaction. This base level is usually taken as mean sea level, but may be re-evaluated to account for paleo-bathymetric and eustatic corrections. Within this method, eroded volumes may be estimated and incorporated into decompaction calculations.

In one dimension, to calculate the thickness of a sediment layer at any time in the past, the layer is moved up the appropriate porosity-depth curve. In other terms, overlying sediment layers are sequentially removed, allowing the layer of interest to decompact from depth interval $[Z_1, Z_2]$ to uncompacted interval $[Z_1', Z_2']$. In the case of exponential relationship between porosity and depth (Eq.1), the decompaction equation, representing the sliding of the sediment layer up the exponential porosity-depth curve is expressed as follows, and is solved using a numerical iterative computation [Allen and Allen, 2005].

$$Z_2'-Z_1' = Z_2-Z_1-\frac{\phi_0}{c}(\exp(-cZ_1)-\exp(-cZ_2))+\frac{\phi_0}{c}(\exp(-cZ_1')-\exp(-cZ_2'))$$
$$(2)$$

To apply decompaction on a volumetric mesh, this equation is used to compute the displacement on each mesh node: decompaction is computed at each point as a function of depth below the surface and below the top of the current layer. This computation is performed starting with the uppermost unit and descending through the lower units so that the displacement of the nodes belonging to the overlying regions is taken into account. Moreover,
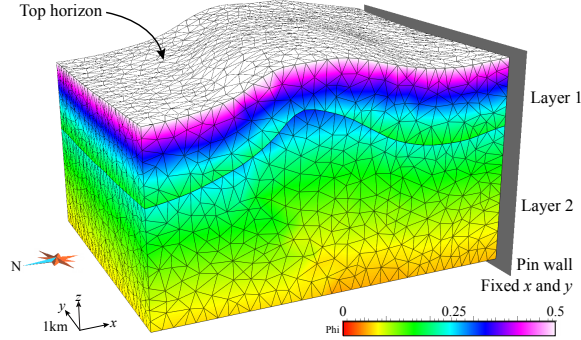
Figure 4: Initial synthetic model displaying porosity as a property and boundary conditions used for first restoration: a pin wall is defined and the top horizon will be restored to a reference elevation (flat datum).

when faults are present in the model, special care must be taken to ensure the continuity of the decompaction. As shown in Fig.3, nodes located "under" the fault are decompacted using the fault surface as top region, which requires the timing and amount of displacement on the fault to be known. For efficiency, we compute fault displacement first by projecting vertically through the layers until reaching the restored surface; then the whole model can be decompacted using the approach illustrated in Figure3B.

In the case of eroded layers, the implicit approach uses several scalar fields for each conformable sequence, thereby providing a possible layer geometry in the eroded area. As done in 3D restoration, decompaction can use this extrapolated geometry to account for initial volumes and thicknesses of sedimentary layers.

4.2 Results on a synthetic growth fold

A synthetic growth fold (Fig.4) was restored, then decompacted. This model was compared with the restored only model. The same boundary conditions were used for both: a wall was fixed along the x and y axes, and a zero reference elevation was defined for the topmost horizon. For the porosity, the layers were considered as shaly sands (layer 1) and sandstones (layer 2).

As shown in Figure5, taking into account decompaction during restoration led to volume changes. The restored and decompacted volume showed a volume difference of 2.3% compared to the restored only model after the first restoration step, and of 1.2% after the second restoration step. Denoting V_0 as the initial volume of the layer and V_i as its volume at a later time i, it is possible to define the compaction rate τ of a layer as the volume ratio:

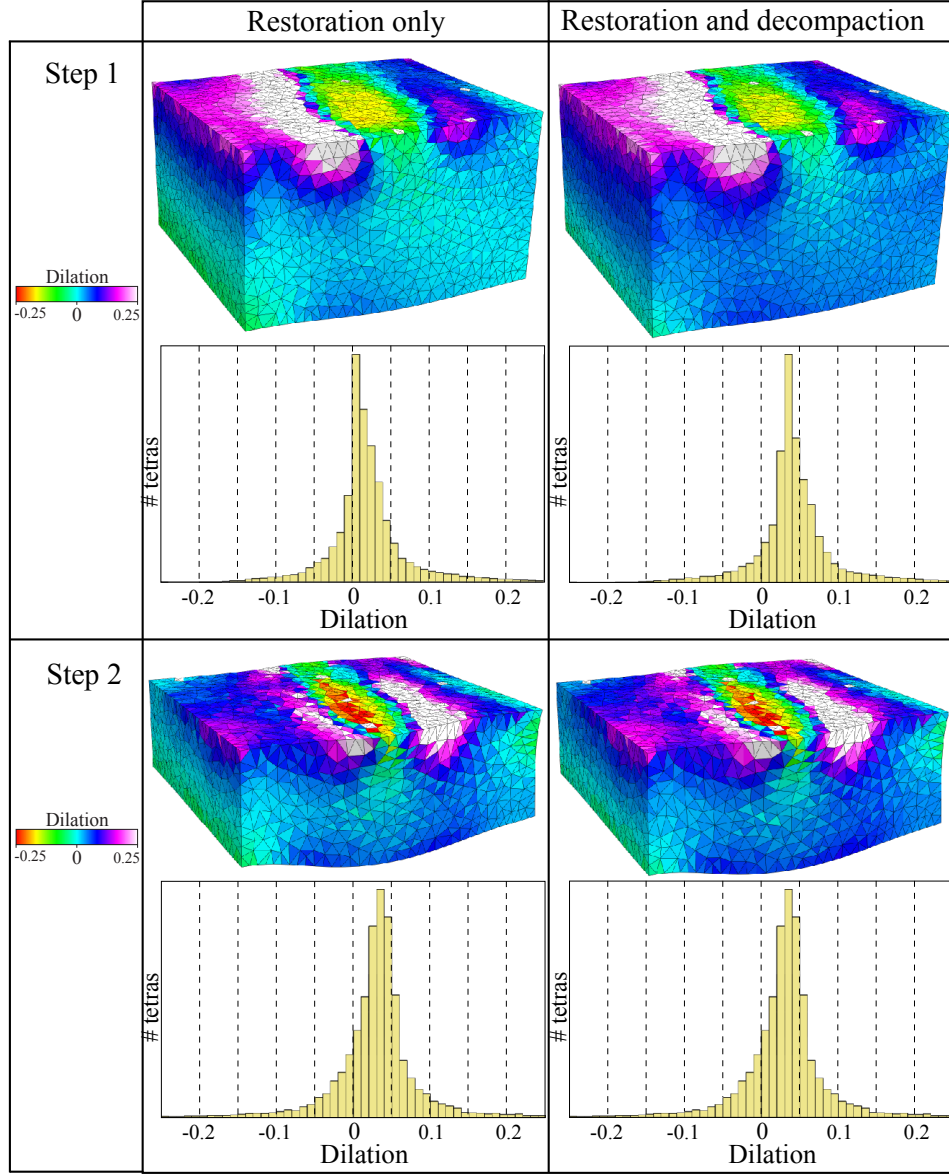$$\tau = \frac{V_i - V_0}{V_0} \tag{3}$$

8

Figure 5: Comparison of restored models with restored and decompacted models, all painted with respective dilation. The histograms of the dilation property are computed and show an increase of the dilation values when the decompaction is performed.
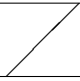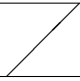
9

Layer	Lithology	Volumes (Gm^3) and volume variation (%)				
		Initial	R. 1	R. & D. 1	R. 2	R. & D. 2
1	Shaly sandstone	393.1 0	397.7 1.2	403.9 1.6	/	/
2	Sandstone	853.7 0	854.5 0.1	877.2 2.8	882.3 3.4	893.0 4.6

Table 1: Volumes and decompaction rates (τ) for the different steps of the backstripping: R. i is the restored only model for the step i, and R. & D. i is the restored and decompacted model for the step i.

Assuming a maximum burial depth of 1000 m for the topmost layer of the model, the compaction was equal to 1.6% for the shaly sandstone layer, and 4.6% for the sandstone layer (Table 1). These results are in agreement with standard estimations of compaction [Sclater and Christie, 1980, Meckel et al., 2007]. For each step of restoration and decompaction, the strain was computed from the summed displacement vectors and the dilation is displayed in Figure 5. Performing decompaction increases the dilation values: the histograms of the dilation property are translated to the right for the decompacted models compared to the restored only models. It is thus important to perform this step separately to have an increased knowledge of the deformation history.

5   Application to the Annot sandstone

5.1   Geological settings

The Annot Sandstone is a well-known analogue for sand-rich deep-water reservoirs [Moraes et al., 2004] that has been studied by many authors [Pickering and Hilton, 1998, Sinclair, 2000, Joseph et al., 2000]. It is preserved in a series of isolated outliers of the Tertiary foreland basin in the Alpine fold-and-thrust belt (SE France). In this case study, we consider the Annot inlier in which the Annot Sandstone is preserved in a growth syncline. It is 70 km NW of Nice (on the Mediterranean coast) and covers an area of 70 km^2 (about 11 km North-South by 6 km East-West). It lies just at the intersection of the Digne thrust system (trending NNW-SSE) and the Castellane Arc (trending E-W) (Fig. 6). In this mini-basin, a turbidite succession fed from the South by fan-deltas was deposited over a period of 10 My from the Bartonian to the Rupelian, in the active Alpine wedge-top foreland basin [DeCelles and Giles, 1996, Ford, 2004]. These turbidite deposits overlie the transgressive Nummulitic Limestone and the deep-water Globigerina Marls. In the Annot depocentre, local members are defined and mapped within this turbiditic formation. They are labelled from A to G upward. The facies

evolve from sand sheet deposits (A and B; distal lobe) to slumps (C and D) and to channelized systems (E, F and G) (Fig. 7).

5.2 Model description

The 3D model was built from available field data [Albussaïdi and Laval, 1984, Callec, 2001, Puigdefàbregas et al., 2004, Salles et al., 2010], taking into account three faults, including the Rouaine fault, in a domain of interest limited by the Ourgues fault towards the East. Two scalar fields were interpolated to model this Tertiary depocentre: one for members A-G, and another one for the Nummulitic Limestone and the Globigerina Marls (Fig.8).

5.3 Used parameters

For the porosity, since no borehole has been drilled in the area, we propose to set typical default values used in most modelling packages (e.g. Sclater and Christie's depth-porosity relationship) and values as described in Figure 2, with a sandstone value for the Annot Sandstone (members A to F), marls and limestone values, respectively for Globigerina Marls and Nummulitic Limestone. The obtained initial porosity ranges from 0.15 to 0.5 % (Fig.9).

The maximum burial depth of the Annot Sandstone is not well documented. It is suggested to have been between 900 and 1200 m for the top of the Globigerina Marls [Mougin, 1978, Euzen et al., 2004]. We use an average value of 1000 m in our study. At each restoration step, the top of the considered layer was restored to $Z = 0$, starting with member G, and the coordinates along the eastern boundary of the model are used as reference. Decompaction was applied on all underlying units between the restoration steps.

Additionally, for comparison purposes, decompaction was computed on two fictitious wells in two different blocks of the model (Fig.11).

5.4 Decompaction impact on restored models

Fig.10 shows the results of two steps of restoration and decompaction. For each step, the restored and decompacted models are shown (respectively R and RD). At the first step, the top of the member G was considered. As expected theoretically, the decompaction led to an increase of dilation values, and differences between the R_g and RD_g models increased with depth. Because this first stage uses the maximum burial depth values to compute decompaction, the obtained values were relatively high, leading to considerable differences between R_g and RD_g configurations. Restoration and decompaction were then performed sequentially on the other layers, using the obtained depth from the previous step. The second step in Fig.10 (R_b and RD_b) corresponds to the restoration and decompaction of the top of member B. The decompaction increased the dilation values as well, but in a way
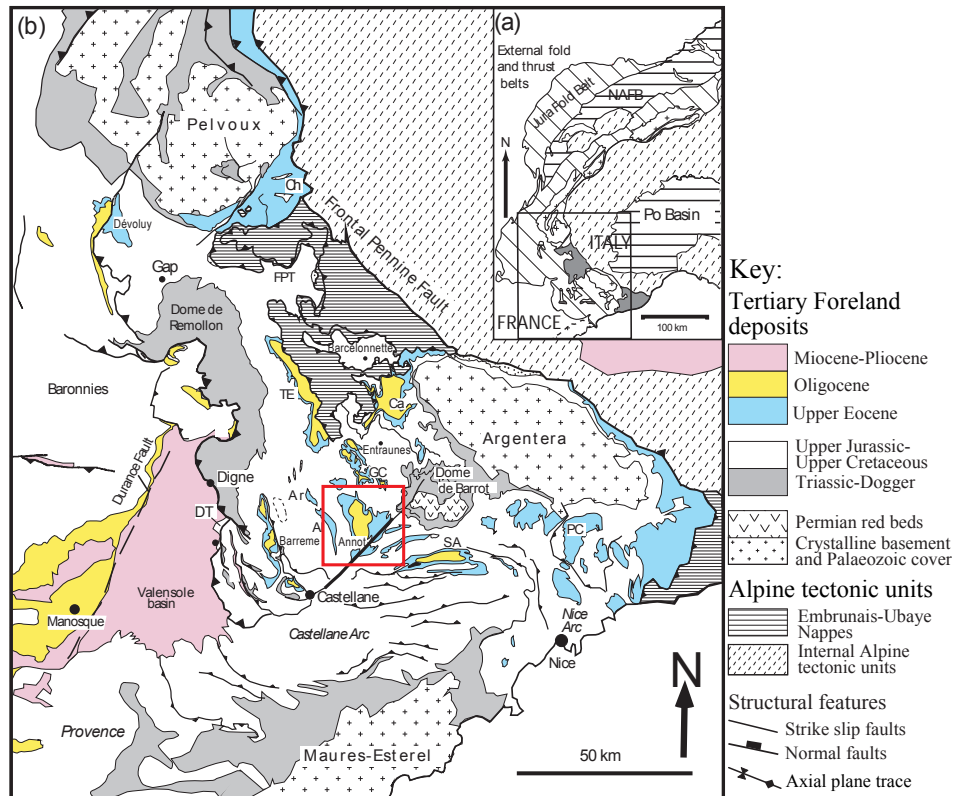
11

Figure 6: a) Simplified geological map of the western Alps showing principal tectonic units. Abbreviation NAFB is Northern Alpine Foreland Basin. b) Regional tectonic map of SE France showing the outliers of the Tertiary Alpine foreland basin. The Annot depocentre is boxed. Abbreviations are as follows: Al, Allons; An, Annot; Ar, Argens; Ca, Cayolle; Ch, Champsaur; DT, Digne Thrust; FPT, Frontal Pennine Thrust; GC, Grand Coyer; PC, Peira Cava; SA, Saint Antonin; TE, Trois Evêchés. Modified from Salles et al. [2010].
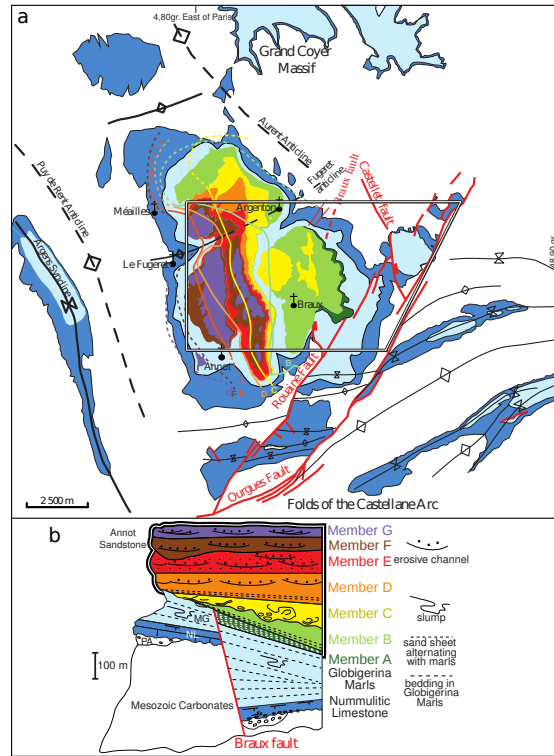
Figure 7: a. Geological map showing the Tertiary stratigraphy and structure of the Annot depocentre. The Annot Sandstone turbidite members A to G onlap progressively westward onto the Globigerina Marls. Colored lines represent western onlap limits of these members. The area analysed in the 3D model is boxed. b. Lithostratigraphy of the Tertiary foreland basin of SE France (Nummulitic trilogy). The Braux normal fault, sealed by the member B, strongly controlled deposition of the Nummulitic Limestone and the Globigerina Marls. Modified from Salles et al. [2010].
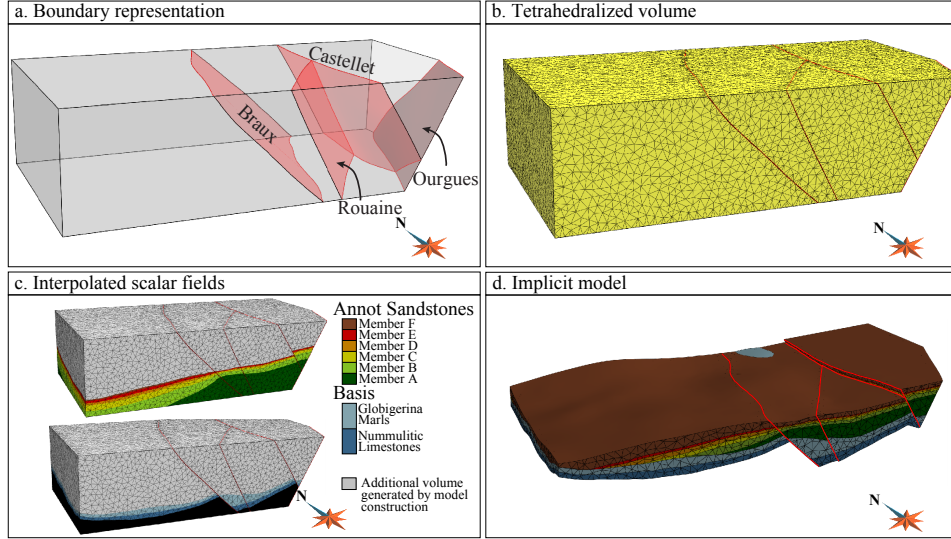
13

Figure 8: Initial model of Annot. a. Boundary representation of the volume of interest, with the associated faults. b. Corresponding tetrahedral mesh. c. Two interpolated properties, the first one corresponding to turbiditic members A to G; the second one to the Globigerina Marls and Nummulitic Limestone. d. Combined view of the present-day 3D stratal geometry, displaying stratigraphic properties in respect with the stratigraphic column.
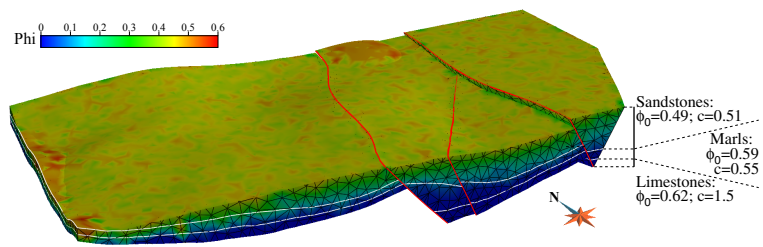

Figure 9: Initial model of the Annot depocentre displaying the porosity property (ϕ), computed from the indicated coefficients of compaction (c) and surface porosity (ϕ_0), per layer, considering the top layer as the reference surface, after moving the model down to a supposed maximum burial depth equal to 1000 m.

that was not significant compared to the uncertainties due to the restoration parameters.

During the whole sequential decompaction process, the dip of the fault surfaces rotated about 1°-2°, compared to the initial model. The connections between the different stratigraphic units across the faults were modified when the dip of the fault was modified. For instance, impermeable rocks of the Globigerina Marls were juxtaposed with Annot Sandstones, sealing the fault where transmissivity was considered possible. Alternative fluid migration pathways can therefore be identified by coupling restoration and decompaction.

5.5   Restoration value in the decompaction process

The plots of depth versus time were drawn on two fictitious wells, one located in the Western fault block and the other one in the Eastern fault block (Fig.11). They show that applying decompaction on wells in the classical way may lead to different decompaction curves as compared to decompacting within the restoration process. The depth variations from the restoration results identify an uplift of member A and of underlying units around 34 Ma. This uplift led to the exposure of some areas of member A above sea level, which should have resulted in erosion. While an uplift can be consistent with the local tectonic setting and with the Sandstone members' lithostratigraphy (members A and B show evidence of a passive basin infill whereas members C-F lithologies highlight an active infill), member A does not show any evidence of erosion. This inconsistency may be due to the restoration to a $Z = 0$ datum: the paleobathymetry during the deposition of members A and B sandstones was not zero. By simply applying decompaction on wells, this specific local tectonic event could not have been detected, in particular in the western block where member A is not present everywhere.

To highlight the importance of an improved burial history, let us assume that the conditions equivalent to the hydrocarbon kitchen were reached at a depth between 400 and 1200 m. Applying backstripping on wells in the classical way, the decompaction graph of the well 1 suggests that member A of the Annot Sandstone was under appropriate conditions for hydrocarbon maturation during more than one million years. Using decompaction and restoration, this period is reduced to about 0.2 m.y., which drastically decreases the timing for hydrocarbon maturation.

6   Conclusions

Coupling sequential restoration and decompaction calculations considerably improves 3D basin analysis. Indeed, taking decompaction into account affects the retro-dilation distribution, which may otherwise be under-estimated.
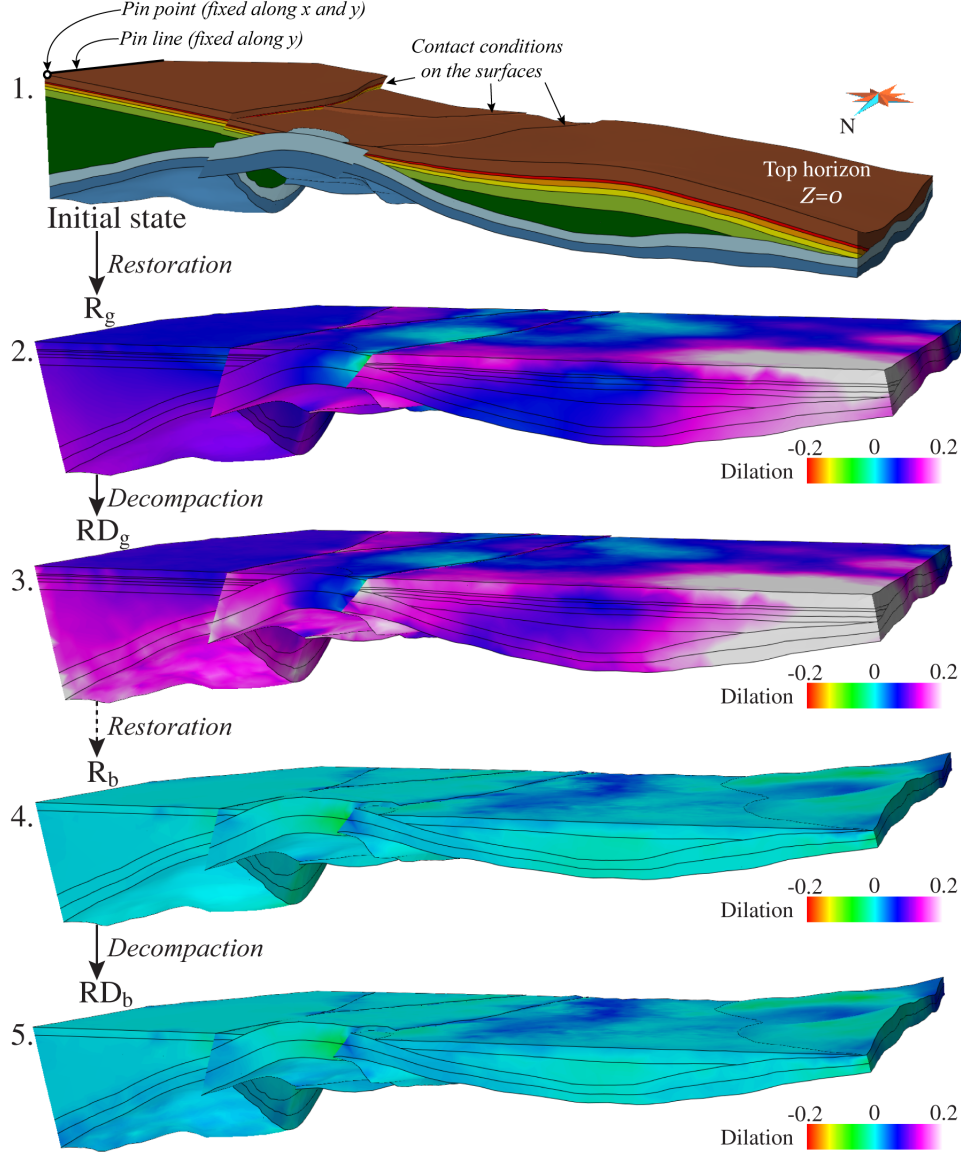
Figure 10: 1. Initial model with boundary conditions for restoration; 2. Results of restoration of the top of member G, showing a tilting of the model; 3. Results of restoration followed by decompaction. The dilation property is computed and painted on R_g using the restoration vectors, and on RD_g using the total vectors (summed restoration and decompaction). 3. and 4. show restoration R_b and restoration followed by decompaction RD_b for a later stage (restoration of the top of member B).
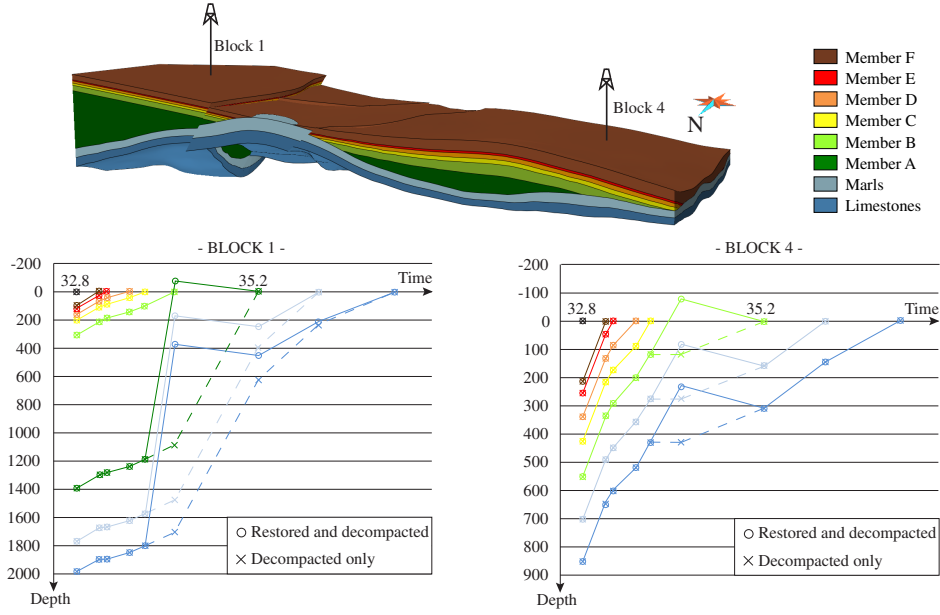
Figure 11: Top. Initial model with the location of the two fictitious wells; Bottom. Plots of depth versus time for the two wells, comparing decompaction at well with decompaction coupled with restoration.

Even if porosity values cannot be calibrated since no borehole data are available in the Annot basin, accounting for decompaction using typical default values allows for an improved assessment of the basin history. A key result of the 3D sequential restoration is the apparent uplift of the lowermost units (member A of the Annot Sandstone, Globigerina Marls and Nummulitic Limestone) which has been identified, while one-dimensional decompaction cannot assess such depth variations. Coupling decompaction and restoration may lead to a better understanding of hydrocarbon maturation and migration. The relationship between porosity and depth has been considered exponential; other relationships (such as linear) could be implemented to quantify related uncertainties. Sensitivity studies of the decompaction coefficient and surface porosity may also be performed to evaluate the impact of using default values in the application to the Annot Sandstone model.

Acknowledgements

17

who initiated the development of the decompaction code, is thanked for his work.

References

S. Albussaïdi and A. Laval. *Nouvelles observations de la série Priabonienne. Evolution latérale en relation avec la tectonique.* M.Sc. dissertation, Ecole Nationale Supérieure du Pétrole et des Moteurs, Rueil-Malmaison, France, 86 pp, 1984.

P. A. Allen and J. R. Allen. *Basin Analysis: Principles and Applications*, chapter Subsidence and Thermal History, pages 349–401. Blackwell publishing, 2nd edition, 2005.

L. Athy. Density, porosity, and compaction of sedimentary rocks. *American Association of Petroleum Geologists Bulletin*, 14:1–24, 1930.

G. Atwater and E. Miller. The effect of decrease in porosity with depth on future development of oil and gas reserves in South Louisiana. *American Association of Petroleum Geologists Bulletin*, 49:334–334, 1965.

Y. Callec. *La déformation synsédimentaire des bassins paléogènes de l'arc de Castellane.* Ph.d., Ecole des Mines de Paris, Paris, France, 674 pp, 2001.

G. Caumon, C. Antoine, and A.-L. Tertois. Building 3D geological surfaces from field data using implicit surfaces. In *Proceedings 27th Gocad Meeting, Nancy, France*, pages 1–6, 2007.

R. Chamberlin. The appalachian folds of central pennsylvania. *Journal of Geology*, 18:228–251, 1910.

C. D. A. Dahlstrom. Balanced cross sections. *Canadian Journal of Earth Sciences*, 6:743–757, 1969.

M. R. De Santi, J. L. E. Campos, and L. F. Martha. A finite element approach for geological section reconstruction. In *Proceedings 22th Gocad Meeting, Nancy, France*, pages 1–13, 2002.

P. DeCelles and K. Giles. Foreland basin systems. *Basin Research*, 8:105–123, 1996.

G. Dickinson. Geological aspects of abnormal reservoir pressures in Gulf Coast Louisiana. *American Association of Petroleum Geologists Bulletin*, 37:410–432, 1953.

P. Durand-Riard. *Gestion de la complexité géologique en restauration géomécanique 3D.* Ph.D. dissertation, Institut National Polytechnique de Lorraine, 150 pp, 2010.

P. Durand-Riard, G. Caumon, and P. Muron. Balanced restoration of geological volumes with relaxed meshing constraints. *Computers & Geosciences*, 36(4):441, 542, 2010.

T. Euzen, P. Joseph, E. D. Fornel, S. Lesur, D. Granjeon, and F. Guillocheau. Three-dimensional stratigraphic modelling of the Grès d'Annot system, Eocene-Oligocene, SE France. *Geological Society Special Publications*, 221: 161–180, 2004.

M. Ford. The significance of growth structures in foreland basin development. *Basin Research*, 16:361–375, 2004.

A. Fowler and C. Noon. Mathematical models of compaction, consolidation and regional groundwater flow. *Geophysical Journal International*, 136: 250–260, 1999.

T. Frank, A.-L. Tertois, and J.-L. Mallet. 3D reconstruction of complex geological interfaces from irregularly distributed and noisy point data. *Computers & Geosciences*, 33(7):932, 943, 2007.

A. Gibbs. Balanced cross section construction from seismic sections in areas of extensional tectonics. *Journal of Structural Geology*, 5(2):153–160, 1983.

J. P. Gratier and B. Guillier. Compatibility constraints on folded and faulted strata and calculation of total displacement using computational restoration (unfold program). *Journal of Structural Geology*, 15(3-5):391–402, 1993.

R. Groshong. *3D Structural Geology: A Practical Guide To Surface And Subsurface Map Interpretation*, chapter Structural validation, restoration and prediction, pages 305–372. Springer Verlag, Berlin Heidelberg, 1999.

M. Gutierrez and M. Wangen. Modeling of compaction and overpressuring in sedimentary basins. *Marine and Petroleum Geology*, 22:351–363, 2005.

H. Hedberf. Gravitational compaction of clays and shales. *American Journal of Science*, 31:241–278, 1936.

K. A. Hegarty, S. S. Foland, A. C. Cook, P. F. Green, and I. R. Duddy. Direct measurement of timing: Underpinning a reliable petroleum system model for the Mid-Continent rift system. *American Association of Petroleum Geologists Bulletin*, 91(7):959–979, 2007.

M. Hölzel, R. Faber, and M. Wagreich. DeCompactionTool: Software for subsidence analysis including statistical error quantification. *Computers & Geosciences*, 34:1454–1460, 2008.

P. Joseph, N. Babonneau, A. Bourgeois, G. Cotteret, R. Eschard, B. Garin, O. Gomes De Souza, D. Granjeaon, F. Guillocheau, O. Lerat, J. Quemener, and C. Ravenne. The Annot Sandstone outcrops (French Alps: architecture description as input for quantification and 3D reservoir modelling). In P. W. et al., editor, *Deep-Water Reservoirs of the World*, SEPM Special Publications, pages 422–449. 2000.

I. Lerche. *Basin Analysis : Quantitative Methods*, volume 1, chapter Applications of Fluid Flow, Compaction, and Thermal Indicators to Single-Well and Basinal Settings, pages 246–345. San Diego: Academic Press, 1990a.

I. Lerche. *Basin Analysis: Quantitative Methods*, volume 2. San Diego: Academic Press, 1990b.

L. Maerten and F. Maerten. Chronologic modeling of faulted and fractured reservoirs using geomechanically based restoration: Technique and industry applications. *American Association of Petroleum Geologists Bulletin*, 90(8):1201–1226, 2006.

K. Magara. Thickness of removed sedimentary rocks, paleopore pressure and paleotemperatures, Southwestern part of Western Canada Basin. *American Association of Petroleum Geologists Bulletin*, 60:554–565, 1976.

K. Magara. Comparison of porosity-depth relationships of shale and sandstone. *Journal of Petroleum Geology*, 3:175–185, 1980.

A. Maillard, V. Gaullier, B. C. Vendeville, and F. Odonne. Influence of differential compaction above basement steps on salt tectonics in the Ligurian-Provençal Basin, Northwest Mediterranean. *Marine and Petroleum Geology*, 20(1):13–27, 2003.

M. Makhous. *Formation of Hydrocarbon Deposits in the North African Basins*, chapter Reservoir Decompaction and Formation of Accumulation Capacity (in secondary porosity) of reservoir rocks, pages 131–183. Berlin: Springer, 2000.

D. McKenzie. Some remarks on the development of sedimentary basins. *Earth and Planetary Science Letters*, 40(1):25–32, 1978.

T. A. Meckel, U. S. Ten Brink, and S. J. Williams. Sediment compaction rates and subsidence in deltaic plains: numerical constraints and stratigraphic influences. *Basin Research*, 19(1):19–31, 2007.

M. A. S. Moraes, P. R. Blaskovski, and P. Joseph. The gres d'annot as an analogue for brazilian cretaceous sandstone reservoirs; comparing convergent to passive-margin confined turbidites. *Geological Society Special Publications*, 221:419–436, 2004.

I. Moretti. Working in complex areas: New restoration workflow based on quality control, 2D and 3D restorations. *Marine and Petroleum Geology*, 25:202–218, 2008.

I. Moretti, F. Lepage, and M. Guiton. Kine3D: a new 3D restoration method based on a mixed approach linking geometry and geomechanics. *Oil & Gas Science and Technology*, 61(2):277–289, 2006.

C. Mougin. *Contribution à l'étude des sédiments tertiaires de la partie orientale du synclinal d'Annot (Alpes de Haute Provence). Stratigraphie, géochimie, micropaléontologie.* Ph.D. dissertation, Université scientifique et médicale de Grenoble, France, 165 pp, 1978.

P. Muron. *Méthodes numériques 3D de restauration des structures géologiques faillées (3D numerical methods of restoration of faulted geological structures).* Ph.D. dissertation, Institut Polytechnique National de Lorraine, Nancy, France, 145 pp, 2005.

S. Nelskamp, P. David, and R. Littke. A comparision of burial, maturity and temperature histories of selected wells from sedimentary basins in the Netherlands. *International Journal of Earth Sciences*, 97:931–953, 2008.

M. J. Pearson and M. A. Russel. Subsidence and erosion in the Pennine Carboniferous Basin, England: Lithological and thermal constraints on maturity modelling. *Journal of the Geological Society, London*, 157:471–482, 2000.

L. Perez. *Modélisation de la compaction dans les bassins sédimentaires - Mise en évidence d'un comportement mécanique tensoriel.* Ph.D. dissertation, Ecole Nationale des Arts et Métiers, France, 147 pp, 1998.

K. Pickering and V. Hilton. *Turbidite systems of Southeast France.* Vallis Press, London, 229pp, 1998.

C. Puigdefàbregas, J. Gjelberg, and M. Vaksdal. The grès d'Annot in the Annot syncline: outer basin-margin onlap and associated soft-sediment deformation. *Geological Society Special Publications*, 221:367–388, 2004.

D. Rouby. *Restauration en carte des domaines faillés en extension (Map restoration of extensive faulted domains).* Ph.D. dissertation, Université de Rennes I, Rennes, France, 210 pp, 1994.

D. Rouby, H. Xiao, and J. Suppe. 3-D restoration of complexly folded and faulted surfaces using multiple unfolding mechanisms. *American Association of Petroleum Geologists Bulletin*, 84(6):805–829, 2000.

L. Salles, M. Ford, P. Joseph, C. Le Carlier de Veslud, and A. Le Solleuz. Migration of a synclinal depocentre from turbidite growth strata: the

Annot syncline, SE france. *Bulletin de la Société géologique de France*, 182(3), 2010.

J. Schmoker and D. Gautier. Compaction of basin sediments: Modeling based on time-temperature history. *Journal of Geophysical Research*, 94: 7379–7386, 1989.

J. Schmoker and R. Halley. Carbonate porosity versus depth: A predictable relation for South Florida. *American Association of Petroleum Geologists Bulletin*, 66:2561–2570, 1982.

F. Schneider, J.-L. Potdevin, S. Wolf, and I. Faille. Mechanical and chemical compaction model for sedimentary basin simulators. *Tectonophysics*, 263: 307–317, 1996.

J. Sclater and P. Christie. Continental stretching: An explanation of the Post-Mid-Cretaceous subsidence of the central North Sea Basin. *Journal of Geophysical Research*, 85:3711–3739, 1980.

F. Shneider, J. Potdevin, S. Wolf, and I. Faille. Modèle de compaction élasto-plastique et visco-plastique pour simulateur de bassins sédimentaires. *Revue de l'Institut Franças du Pétrole*, 49(2):141–148, 1994.

H. Sinclair. Delta-fed turbidites infilling topographically complex basins: a new depositional model for the Annot Sandstones, SE France. *Journal of Sedimentary Research*, 70:504–519, 2000.

E. Suetnova. Numerical simulation of accumulation of gas hydrates during sedimentation and compaction of sediments under subaqueous conditions. *Physics of the Solid earth*, 43:87–93, 2007.

J. Weller. Compaction of sediments. *American Association of Petroleum Geologists Bulletin*, 43:273–310, 1959.

V. Yarushina and Y. Podladchikov. The effect of non-hydrostaticity on elasto-plastic compaction and decompaction. *Physics of the Solid Earth*, 43(1):67–74, 2007.